Reaction Kinetics, Mechanisms and Catalysis (2024) 137:2231–2252
https://doi.org/10.1007/s11144-024-02659-1

Porous Al_2O_3-pillared bentonite synthesized by sonochemistry and its performance as a catalyst in diethyl ether production via ethanol dehydration

Puji Wahyuningsih[1,2] · Aldino Javier Saviola[1] · Karna Wijaya[1] · Aulia Sukma Hutama[1] · Won-Chun Oh[3] · Latifah Hauli[4]

Received: 19 April 2024 / Accepted: 15 May 2024 / Published online: 22 May 2024
© Akadémiai Kiadó, Budapest, Hungary 2024

Abstract

This research investigated the performance of bentonite and Al-PILC as catalysts in ethanol conversion to diethyl ether through a dehydration reaction. The natural bentonite was intercalated with the pillaring agent Keggin-ion Al_{13} to obtain Al-intercalated bentonite. Al-intercalated bentonite has been synthesized using conventional stirring and ultrasonication. Al-intercalated bentonite was calcined at 400 °C for 4 h to produce Al_2O_3 pillared bentonite (Al-PILC). The dehydration reaction was conducted using a 0.2 g catalyst and 10 mL of ethanol with a nitrogen gas flow rate of 20 mL/min at various reaction temperatures (200, 225, and 250 °C) using a fixed bed microreactor. The characterization results reveal that Al-PILC synthesized by sonochemistry exhibits significantly higher surface area and total acidity values than bentonite and Al-PILC synthesized by conventional methods because of the formation of stable Al_2O_3 pillars in the interlayer spaces of bentonite. The sonochemically synthesized Al-PILC produces optimum ethanol conversion and diethyl ether yield of 46.05% and 41.11%, respectively. The conversion of ethanol and diethyl ether yield reaches an optimum result at 225 °C. Based on this study, the pillarization of bentonite using Al_2O_3 can enhance its catalytic properties toward diethyl ether production.

✉ Karna Wijaya
karnawijaya@ugm.ac.id

[1] Department of Chemistry, Faculty of Mathematics and Natural Sciences, Universitas Gadjah Mada, Yogyakarta 55281, Indonesia

[2] Department of Chemistry, Faculty of Engineering, Universitas Samudra, Aceh 24354, Indonesia

[3] Department of Advanced Materials and Engineering, Hanseo University, Seosan-si, Chungcheongnam-do 31962, Republic of Korea

[4] Research Center for Chemistry, National Research and Innovation Agency (BRIN), The B. J. Habibie Science and Technology Area, South Tangerang, Banten 15314, Indonesia

Graphical abstract

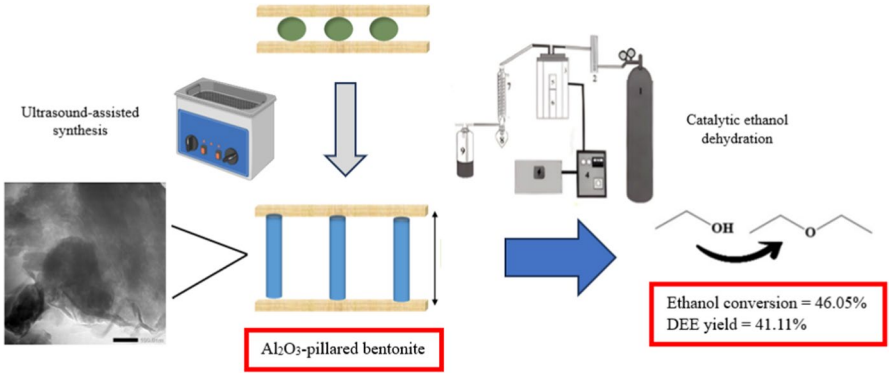

Keywords Al_2O_3-pillared bentonite · Solid acid catalyst · Sonochemistry · Ethanol dehydration · Diethyl ether

Introduction

The availability of sustainable energy reserves and the decrease in pollutants to the surroundings, in the form of emissions produced from fossil fuels, pose challenges for researchers in discovering environmentally friendly renewable energy sources [1]. One promising alternative fuel candidate is diethyl ether (DEE), recognized as a potential oxygenated fuel suitable for ignition in gasoline and diesel engines [2]. This recognition stems from its distinctive characteristics, which include high volatility, low flash point, an octane number exceeding 125, high oxygen content, wide flammability limits, low ignition energy, excellent miscibility with diesel and bioethanol fuels, and minimal carbon monoxide emissions [3–8]. Diethyl ether is used in various applications and is an aromatic solvent alternative; therefore, it plays a crucial role in the fine chemicals sector [9].

Diethyl ether is a product obtained through the dehydration reaction of ethanol using homogeneous acid catalysts, like sulfuric acid, which are toxic and corrosive [10]. However, homogeneous catalysts offer advantages in terms of stability and activity because of their excellent solubility in the reaction medium [11]. Researchers can overcome the drawbacks of homogeneous acid catalysts by employing heterogeneous acid catalysts, which offer advantages such as ease of separation, non-corrosiveness, non-toxicity, cost-effective purification, and environmental friendliness [12]. On an industrial scale, ethanol dehydration is typically performed using solid acid catalysts, with H-ZSM-5 zeolite being the most frequently employed and serving as a reference catalyst [1]. In addition, metal oxides, alumina, silica-alumina, and heteropolyacids have been investigated for their high catalytic activity in ethanol dehydration.

Bentonite is a silica-alumina material containing montmorillonite components with a high swelling ability and cation exchange capacity (CEC) [13]. Consequently, bentonite can accommodate many other metals in the interlayer regions (Al, Zr, Fe, Ti, and Cr). Pillared bentonite (PILC) has emerged as a strong candidate for catalyst support because of its molecular sieve characteristics and resistance to sheet deformation, even at relatively high temperatures. The specific surface and reactant adsorption area is significantly larger than the untreated bentonite [14, 15]. Different metal oxides used as pillaring agents determine the physicochemical characteristics of pillared bentonite [16]. Incorporating mixed metals into the welcomer clay further enhanced the catalytic properties of the PILCs. Keggin ion-Al_{13} is frequently used as a pillaring agent because of its well-defined structure and chemical composition, which produce increased thermal stability and high acidity [17, 18]. Textural and acidity characteristics of the catalyst have a critical role in influencing the catalytic activity [19].

Previous researchers have synthesized Al_2O_3-pillared bentonite using alkaline-hydrolyzed aluminum salt solutions [20–25]. However, the method remains conventional, employing $AlCl_3$ salt under hydrolysis conditions with an OH^-/Al^{3+} mole ratio of 2–2.5, followed by stirring for 24 h. This conventional approach necessitates an extended reaction time and substantial water consumption, making it less effective and efficient for industrial-scale applications. Recent studies have sought to overcome these limitations in the pillarization process by reducing the synthesis costs and exploring environmentally friendly technologies. These alternatives include ultrasonication [16, 26, 27], microwave radiation [28], and one-step high-temperature processes [29, 30].

Ultrasonication is a homogenization technique designed to break down large particles into smaller ones through cavitation waves, resulting in smaller and more uniform particle sizes [27, 31]. Ultrasonic technologies, as one of the synthesis methods, offer the advantage of reducing reaction time, minimizing water and reactant consumption, saving energy, and decreasing waste in pillaring bentonite [32, 33]. This renders ultrasonication an environmentally friendly method that aligns with the principles of green chemistry. Additionally, ultrasonication effectively improves the mass transfer rate between immiscible liquids in a heterogeneous system, generating sufficient activation energy for a reaction [34]. Compared to traditional approaches, the ultrasonication process shows superior physiochemical characteristics regarding catalyst morphology, structure, and surface area. In addition, the ultrasonication method increases the surface area available for the reaction to occur while improving the dispersion of metal particles on the support system and preventing agglomeration [35].

Using ultrasonication, the pillarization process of bentonite takes only 20 min to produce pillared bentonite with the same characteristics as the conventional stirring method for 24 h [36]. The rise in ultrasonic energy would result in smaller and more uniform particle sizes due to the mechanical stress produced by ultrasonication-generated cavitation waves [27]. Ultrasonication also improves the surface characteristics of materials, such as average pore diameter, total pore volume, and specific surface area, by 4 to 6 times. Furthermore, the ultrasonication process for 20 min can increase the specific surface area of Al/Cr-PILC three times more than the

conventional method [32]. Tomul et al. [37] studied the effects of ultrasonic treatment and the traditional method for synthesizing Zr-pillared bentonite modified with Ce. According to the XRD results, the Zr and CeZr-pillared bentonites made conventionally showed basal spacing d_{001} above 3.5 nm, which corresponds to the mesoporous pillared sites and another small basal spacing d_{001} above 1.7 nm that is associated with microporous sites. They also obtained similar results using ultrasonic treatment of Zr and CeZr-pillared bentonites that produce low-intensity basal spacing d_{001} above 1.9 nm.

Pillared bentonite shows promise as a catalyst in diethyl ether synthesis, boasting critical properties such as a substantial surface area, high porosity, robust thermal and hydrothermal stability, and elevated surface acidity. The synthesis of diethyl ether via ethanol dehydration, utilizing an alumina-intercalated vermiculite catalyst, was investigated by Maroszh et al. [38] across a temperature range of 50 to 300 °C. With increasing temperature, the ethanol conversion rate increases, reaching its maximum of 98% under optimal conditions at 300 °C with the alumina-pillared catalyst (Al-PILC). Notably, the Al-PILC catalyst exhibited the highest selectivity for diethyl ether at 72%. Hasanudin et al. [39] studied diisopropyl ether synthesis using molybdenum phosphide pillared bentonite (MoP-PILC) in the dehydration reaction of isopropyl alcohol. The acidity and pore size after pillarization also increased than Na-bentonite. The maximum acidity, ranging from 1.5755 to 5.7732 mmol/g, is found in MoP-PILC 4 mEq/g, suggesting a rise in catalytic activity. The composition of the MoP-PILC catalyst is 4 mEq/g, which produces the maximum diisopropyl ether yield of 64.5%. Hasanudin et al. [40] used zirconium phosphate pillared Na-montmorillonite as the catalyst in a comparable study. Over a temperature range of 150–350 °C, this catalyst produced a methanol conversion rate of 96.76%, a dimethyl ether product yield of 96.8%, and a dimethyl ether selectivity of 93.67% with an LSHV of 2.54 h^{-1} using N_2 gas flow. PILC catalysts demonstrated higher activity than γ-Al_2O_3. γ-Al_2O_3 catalysts showed superior selectivity for diethyl ether products but less selectivity for ethylene than PILC [41].

Therefore, this study emphasizes the green synthesis of Al_2O_3-pillared bentonite using ultrasonication expected to produce a catalyst with high acidity, high activity, and selectivity in the dehydration of ethanol to diethyl ether. This investigation also compares the physicochemical characteristics of Al_2O_3-pillared bentonite prepared with both conventional stirring and ultrasonication at the intercalation stage, such as crystallinity, the change in basal spacing d_{001}, morphology structure, elemental content, surface area, porosity, and total acidity. The catalytic activity of the Al_2O_3-pillared bentonite was evaluated in the synthesis of diethyl ether at various reaction temperatures (200, 225, and 250 °C) using a fixed bed microreactor.

Experimental

Materials

The materials used in this research were commercial Ca-bentonite, aluminum(III) chloride hexahydrate ($AlCl_3{\cdot}6H_2O$, Sigma Aldrich), sodium hydroxide (NaOH, E

Merck), silver(I) nitrate ($AgNO_3$, E Merck), 99% ethanol (C_2H_5OH, Sigma Aldrich), deionized water (CV Bima Aksara Nusa), and nitrogen gas (N_2, PT Surya Indotim Imex).

Bentonite preparation

Bentonite preparation was conducted using the procedure referred to [42]. 50 g of bentonite was washed with deionized water three times. The mixture was centrifuged at 4500 rpm for 30 min to separate the filtrate and residue. The obtained residue was dried at 110 °C for 6 h, ground, and sieved using a 250-mesh sieve.

Synthesis of Al_2O_3-pillared bentonite

Bentonite suspension (2% w/v) was stirred for 24 h at room temperature. 0.2 M NaOH was added slowly to 0.2 M $AlCl_3$•$6H_2O$ with a mole ratio of $OH^-/Al^{3+} = 2.2$, and the mixture was stirred for 24 h at room temperature to produce an Al_{13} pillar solution. The intercalation process is performed by slowly adding the Al_{13} pillar solution to the bentonite suspension. The intercalation process was performed using two methods: stirring for 24 h at room temperature and ultrasonication at 30 °C for 20 min. The mixture was centrifuged at 3500 rpm for 30 min, and the filtrate was neutralized until it was free of chloride ions (Cl^-), as indicated by a negative test for $AgNO_3$). The resulting precipitates were dried at 110 °C for 24 h, ground, sieved using a 250-mesh sieve, and then calcined at 400 °C for 2 h, flowing by N_2 gas with a 20 mL/min flow rate. The obtained solids are Al_2O_3 pillared bentonite (Al-PILC) and labeled as Al-PILC (A) for Al_2O_3 pillared bentonite was intercalated using stirring for 24 h at room temperature and labeled as Al-PILC (B) for Al_2O_3 pillared bentonite was intercalated using ultrasonication at 30 °C for 20 min.

Characterization of the catalysts

The effectiveness of the alumina (Al_2O_3) pillarization process as a pillaring agent was noticeable through alterations in the basal spacing (d_{001}) and crystallinity of the catalyst, as determined by X-ray analysis (Shimadzu XRD-6000) equipped with a Cu X-ray tube (1.5406 Å). The functional groups in the catalyst materials were measured using a Fourier transform infrared (FTIR) instrument (Thermo Scientific Nicolet iS10 at wavenumbers 4000–400 cm^{-1}. Scanning electron microscopy electron dispersive X-ray spectrometry (SEM–EDX) mapping instrument (JEOL JED-2300) and transmission electron microscope (TEM) instrument (JEM-1400 JEOL/EO) were used to examine the morphological structure and elemental composition of the catalyst surface.

The total acidity and acid density of the catalyst materials was determined using the Temperature Programmed Desorption of Ammonia (NH_3-TPD) instrument (Micromeritics Chemisorb 2750), which was heated between 100 and 800 °C at a heating rate of 10 °C/min. The surface area and porosity were analyzed using a Surface Area Analyzer (SAA) instrument (Quantachrome Novatouch LX-4) at

a degassing temperature of 300 °C for 4 h. A thermogravimetric analyzer (TGA) instrument (TGA 5500) was used to characterize the thermal stability of the catalyst at ambient temperatures up to 1000 °C, with a heating rate of 10 °C/min.

Synthesis of diethyl ether via catalytic ethanol dehydration

Diethyl ether was prepared by ethanol dehydration using a fixed-bed microreactor (see Fig. S1) with an inner diameter of 0.5 inches and a length of 30 cm according to the two combined methods [6, 43]. The dehydration reaction was conducted using 0.2 g of catalyst and 10 mL of ethanol at a nitrogen gas flow rate of 20 mL/min. The diethyl ether product was analyzed using gas chromatography–mass spectrometry (GC–MS, Shimadzu QP2010S). The ethanol conversion and diethyl ether yield (%) can be calculated using Eqs. 1 and 2 [40]. Similarly, the reaction temperature for the best catalyst was varied to 200, 225, and 250 °C.

$$\text{Ethanol conversion (\%)} = \frac{\text{m ethanol}_{in} - \text{m ethanol}_{out}}{\text{m ethanol}_{in}} \times 100 \quad (1)$$

$$\text{DEE yield (\%)} = \frac{E_i}{E_{total}} \times 100 \quad (2)$$

Here: m ethanol: mass of ethanol (g); E_i: peak area of DEE in GC chromatogram, E_{total}: total peak area in GC chromatogram.

Results and discussion

X-ray diffraction analysis

The XRD patterns of bentonite, intercalated bentonite, and Al_2O_3 pillared bentonite (Al-PILC) are shown in Fig. 1. The crystal phases in the sample show diffraction peaks corresponding to JCPDS No 13–0135 (montmorillonite), JCPDS No 46–1045 (quartz), and JCPDS No 47–1743 (calcite). The diffractogram of Al-PILC reveals peaks at $2\theta = 19.68°$, 34.65°, and 61.84°, indicating the presence of montmorillonite layers, which are the significant constituents of bentonite. The peak at 26.55° suggests the presence of quartz (SiO_2). The presence of quartz is confirmed by the existence of an absorption peak at 794 cm^{-1}, as indicated in Fig. 2. Al-PILC exhibits a diffraction pattern that is almost identical to bentonite. The diffraction peak of Al-PILC has a relatively lower intensity than bentonite and intercalated bentonite. This suggests that the formation of Al_2O_3 metal oxide is somewhat limited.

The phenomena of Al_2O_3 intercalation and pillarization into the interlayer silicate structure of bentonite can be observed by examining the peak shifts on the (001) plane. In general, the pillarization or intercalation process will cause a change in the low-angle diffraction of d001 and enhance the basal spacing of d_{001} in bentonite. The d_{001} of bentonite, Al-intercalated bentonite, and Al-PILC are 12.49 Å at 2θ

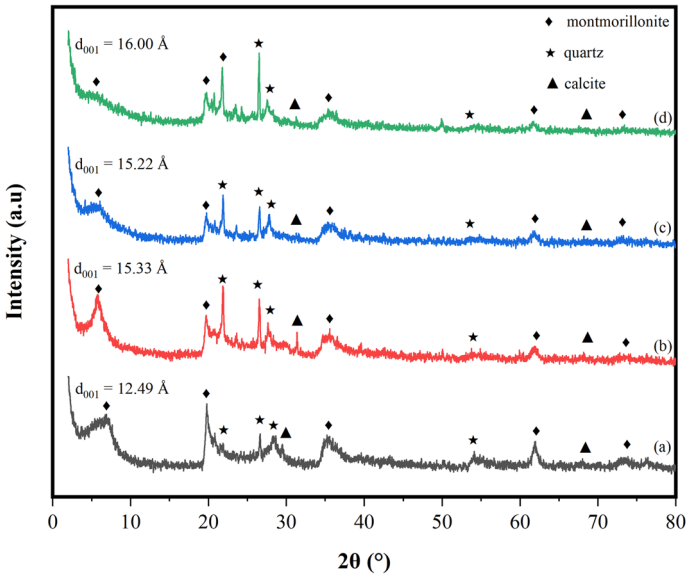

Fig. 1 XRD patterns of **a** bentonite, **b** Al-intercalated bentonite, **c** Al-PILC (A), and **d** Al-PILC (B)

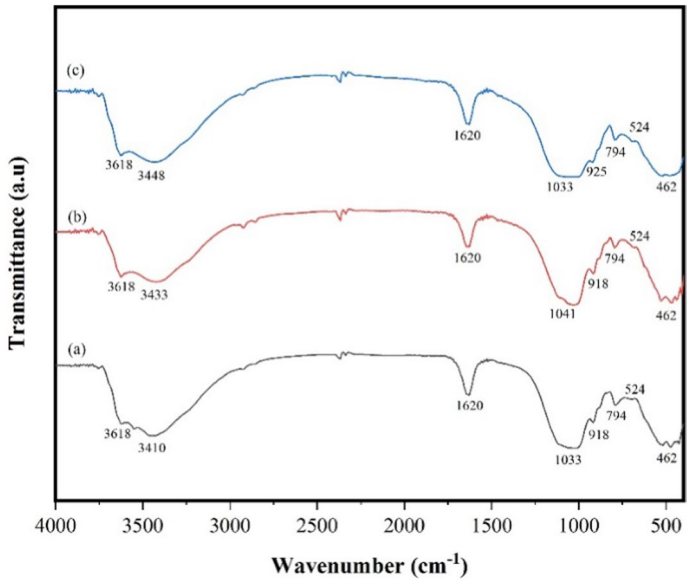

Fig. 2 FTIR spectra of **a** bentonite, **b** Al-PILC (A), and **c** Al-PILC (B)

of 7.07° ($\Delta d_{001} = 2.89$ nm), 15.33 Å at 2θ of 5.76° ($\Delta d_{001} = 5.73$ nm), and 15.22 Å at 2θ of 5.80° ($\Delta_{d001} = 5.63$ nm), respectively. This value represents the distance between two bentonite layer structures, including the thickness of the layer (9.6 Å) [44]. One bentonite layer consists of an alumina silicate layer (two tetrahedral layers

and one octahedral layer) of 9.6 Å, and the distance between the bentonite layers (Δd_{001}) [45], as seen in Fig. S2. The reflection peak shift to lower degrees indicates increased basal spacing in the bentonite after intercalation. This occurs because the larger-sized Keggin-ion Al_{13} replaces the cations present in the interlayer spaces of bentonite (Ca^{2+}, Na^{+}, K^{+}) through a cation exchange mechanism [46]. After the calcination process, the basal spacing decreases because of the dehydration and dehydroxylation processes, forming aluminum metal oxide, which serves as pillars within the interlayer silicate structure of bentonite. The increasing intensity peak of quartz after Al_2O_3 pillarization is likely due to the structural changes induced by the pillarization process. The Al_2O_3 pillars are introduced into the interlayer of bentonite, leading to the expansion of the interlayer spaces and the formation of a more stable structure. This process can reduce the intensity of the characteristic peaks associated with montmorillonite, as the original crystal lattice of the clay mineral may be disrupted or altered. On the other hand, quartz impurities or the exposure of quartz grains on the pillared bentonite's surface may contribute to the increase in quartz peaks.

The intercalation method in the synthesis of Al-PILC also affects the value of basal spacing d_{001} (see Fig. 1). Al-PILC prepared using the ultrasonication method (Al-PILC (B)) results in a peak in the region of $2\theta = 5.88°$ with a basal spacing value of 16.00 Å ($\Delta_{d001} = 3.42$ nm). The peak intensity d_{001} in Al-PILC (B) is lower than in Al-PILC (A). The ultrasonic process facilitates the diffusion of Al_{13}-pillars into clay layers during the exchange process [47]. These results are supported by the smaller average pore size in Al-PILC prepared using sonochemistry (see Table 1) because ultrasonic waves break down large particles into smaller, more uniform particles [27, 31].

Infrared analysis

The FTIR spectra of the bentonite and Al-PILCs are presented in Fig. 2. The absorption peak at wavenumber 3410 cm^{-1} is assigned to the stretching vibration of –OH groups for physisorbed water molecules (H_2O) from silanol (Si–OH) [14, 46, 48] and at 3618 cm^{-1} is assigned to the stretching vibration of –OH groups coordinated to Al^{3+} cations (aluminol) in the octahedral layers (TO_6) on the bentonite structure [49]. The pillarization process replaces many interlayer cations in the form of hydrated compounds, decreasing the intensity of the –OH peak. Therefore, using various synthesis methods, a significant decrease in the peak intensity occurs at

Table 1 Surface and pore characteristics of the catalysts

Sample	Specific surface area (m^2/g)	Total pore volume (cc/g)	Average pore diameter (nm)
Bentonite	47.53	0.10	8.69
Al-PILC (A)	54.54	0.10	7.16
Al-PILC (B)	60.03	0.11	7.14

3410 cm^{-1} for Al-PILC materials. This result is likely due to aluminum metal oxide (Al_2O_3) pillars forming within the bentonite structure.

The high intensity of a band observed at 1630 cm^{-1} represented the bending vibration of hydroxyl and absorbed interlayer water molecules within the host clay [50]. However, its intensity diminished in the pillared clay due to the replacement of larger hydrated interlayer cations [51]. The Si–O–Si stretching vibration occurred at 1033 cm^{-1} and shifted to 1041 cm^{-1} after pillarization due to the formation of Al_2O_3 in interlayer spaces of bentonite. At the wavenumber of 918 cm^{-1}, a peak is related to the bending vibration of Al–Al–OH. The absorption intensities of Si–O bending vibration from quartz minerals (SiO_2) and Si–O–Si bending vibrations in the tetrahedral layer (TO_4) are detected at 794 cm^{-1} and 462 cm^{-1}, respectively [48, 52], and their intensity was decreased in Al-PILC materials. The peak at 794 cm^{-1} is the bentonite impurities, which do not undergo significant changes for the Al-PILC catalyst prepared without ultrasonication.

Surface area and porosity analysis

The N_2 adsorption–desorption isotherm profiles for bentonite, Al-PILC (A), and Al-PILC (B) are shown in Fig. 3. According to the IUPAC classification, the N_2 adsorption–desorption isotherm profiles of bentonite and Al-PILCs are type IV, indicating the formation of mesoporous materials. A material is claimed to be mesoporous if it has pore diameters between 2 and 50 nm. The profiles also display the hysteresis loop H4, which is typical of narrow slit-like pores and is observed in the P/P_0 range

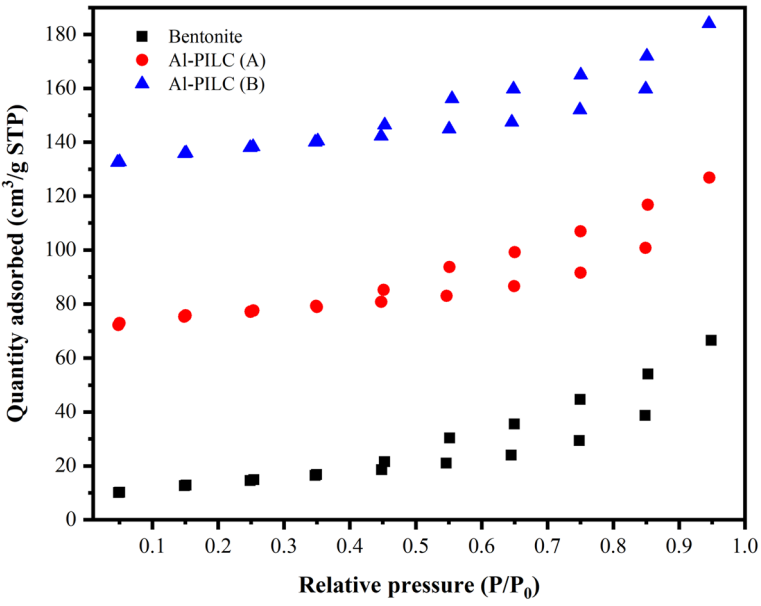

Fig. 3 N_2 adsorption–desorption isotherm profiles of the catalysts

of 0.45–1.0. The pore sizes obtained in bentonite and Al-PILCs with the highest frequency range of 4–5 nm supported their classification as mesoporous materials (see Fig. S3). The pore size distribution curve of both the bentonite and Al-PILC materials dominated the mesoporous sizes (2–50 nm) and did not show pore distribution in the micropore range (< 2 nm).

The pillarization process using Al_2O_3 alters the surface characteristics of bentonite (see Table 1). The specific surface area (SBET) increases because of the intercalation of the Keggin-ion Al_{13} into the interlayer structure of bentonite, even though the average pore diameter decreases. The reduction in the average pore diameter of Al-PILCs could be attributed to the aluminum cations filling the pores during the exchange process in the intercalation stage. The bentonite layer arrangement changes from a delaminated structure (house of cards) to a more regular, face-to-face interaction, contributing to decreased average pore diameter. The results indicate that the surface area and total pore volume of the Al-PILC catalyst synthesized by sonochemistry are higher than those of the conventional method, and there is a decrease in average pore diameter, although this is significant. The change in pore size occurs due to cavitation waves generated by ultrasonication [27].

The mechanism of bentonite pillarization using Al_2O_3 is shown in Fig. 4. The pillarization process is based on the swelling phenomenon in bentonite, where the distance between the bentonite layers increases after hydration (d_1). The pillarization process in bentonite consists of two main stages: intercalation and calcination. The intercalation stage involves inserting polyhydroxy metal cations into the interlayer space of bentonite through a cation exchange mechanism. In contrast, the calcination stage is the stage of forming metal oxides by heating at high temperatures. However, the layered structure of bentonite collapses upon dehydration. The initial stage of bentonite pillaring involves the intercalation of bentonite using a large-sized aluminum polycation with a high charge, namely the Keggin-ion ($[AlO_4Al_{12}(OH)_{24}(H_2O)_{12}]^{7+}$), which replaces Na^+, K^+, or Ca^{2+} ions between

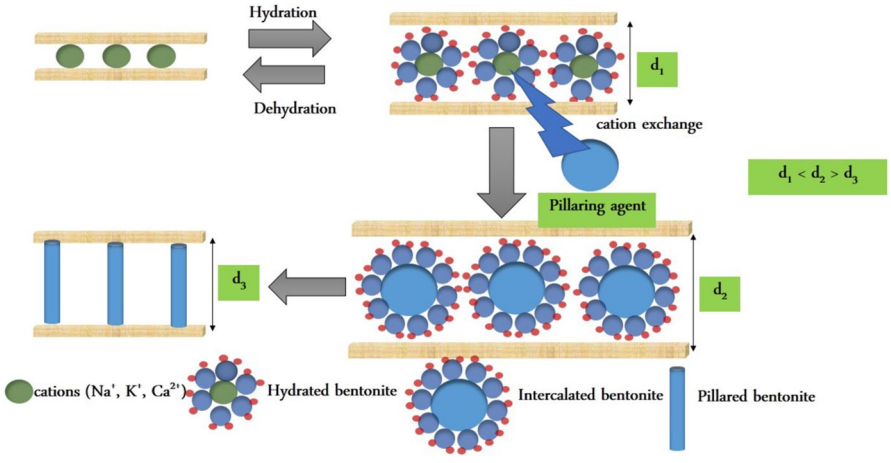

Fig. 4 Mechanism of bentonite pillarization by Al_2O_3

bentonite layers through a cation exchange mechanism. As a result, the distance between the bentonite layers increases (d_2). Subsequently, during the calcination process, the Keggin-ion undergoes dehydration and dehydroxylation, forming aluminum oxide metal pillars (Al_2O_3) that open and support the structure between the bentonite layers (d_3). The pillaring phenomenon causes intercalated bentonite (d_2) to have a greater distance between layers than hydrated bentonite (d_1) and pillared bentonite (d_3).

Morphological and elemental composition study

SEM images are shown in Fig. S4, where Al-PILC obtained through ultrasonication during the pillarization exhibit small particles with sizes identical to those obtained without ultrasonication. In contrast, pillared bentonite without ultrasonication typically exhibits large aggregates or bulky particles. Ultrasonication-assisted pillarization produced small, uniform particles in the bentonite layers. Because of the significant accumulation of particles, the ultrasonication effect can perforate them, forming small porous particles [53]. Consequently, the surface area of the Al-PILC catalyst was higher in the presence of ultrasonic treatment (see Table 1).

The distribution of the elements in bentonite before and after the pillarization process using EDX is shown in Table 2, and the elemental mapping of the Al-PILC (B) catalyst is shown in Fig. S5. The type of bentonite used in this research is Ca-bentonite. After the pillarization process, the amount of aluminum increased, but the quantity of the other elements (Si, Ca, Mg, and Fe) decreased. In Al-PILC (A), the aluminum content increased from 5.53% to 6.32%, and the calcium and magnesium contents decreased from 1.14% to 0.41% and from 3.24% to 0.63%, respectively. This is because of the exchange process between the cations in the interlayer spaces of bentonite, such as Ca^{2+} or Mg^{2+}, with the metal polycation Al_{13} in the pillaring solution.

The same results were obtained for the Al-PILC (B) catalyst prepared by ultrasonication. The amount of aluminum in Al-PILC (B) is significantly higher than that in Al-PILC (A) (without ultrasonication), with values of 7.83% and 6.32%, respectively. The sonochemical synthesis of Al_2O_3-pillared bentonite using ultrasonic waves provides a more effective cation exchange process between the pillaring agent and interlayer cations in the bentonite structure than without the

Table 2 Elemental composition (wt%) obtained by EDX of bentonite, Al-PILC (A), and Al-PILC (B)

Element	Bentonite	Al-PILC (A)	Al-PILC (B)
O	55.90	44.30	46.80
Al	5.53	6.32	7.83
Si	18.81	11.92	12.65
Ca	1.14	0.41	0.59
Mg	3.24	0.63	0.65
K	0.30	0.59	0.62
Fe	5.89	1.79	1.56

ultrasonication process. Therefore, the quantity of metal to be exchanged with cations in the interlayer regions of bentonite by the ultrasonication process is much higher than that without ultrasonication.

The TEM micrographs of bentonite and Al-PILC are presented in Fig. S6. The lamellar structure of bentonite material is more apparent than in SEM micrographs. The parallel lines depict the bentonite's layered structure, which becomes apparent following the alumina oxide pillarization process. The Al-PILC catalyst shows a larger sheet structure than bentonite due to the pillaring process of aluminum metal oxide. This process enlarges the interlayer space of bentonite that resulted from the intercalation of aluminum polycations into the bentonite interlayer, as indicated by an increase in the basal spacing d_{001} after pillarization and enhancement of the surface area, as can be seen in Table 1.

Acidity study

NH_3-TPD examines the total acidity of all catalysts between 100 and 800 °C, as shown in Fig. 5. There are two desorption ranges in the TPD profiles, i.e., the desorption peak at lower temperatures below 300 °C (weak acid sites) and higher temperatures above 300 °C (strong acid sites). Note that the pillarization of bentonite with Al_2O_3 causes an increase in the desorption peak at lower and higher temperatures, indicating that Al_2O_3-pillared bentonites have significantly higher acidity than bentonite. This suggests that the intercalation of Al_2O_3 into the bentonite structure results in stronger physical ammonia adsorption on the pillared bentonite surface.

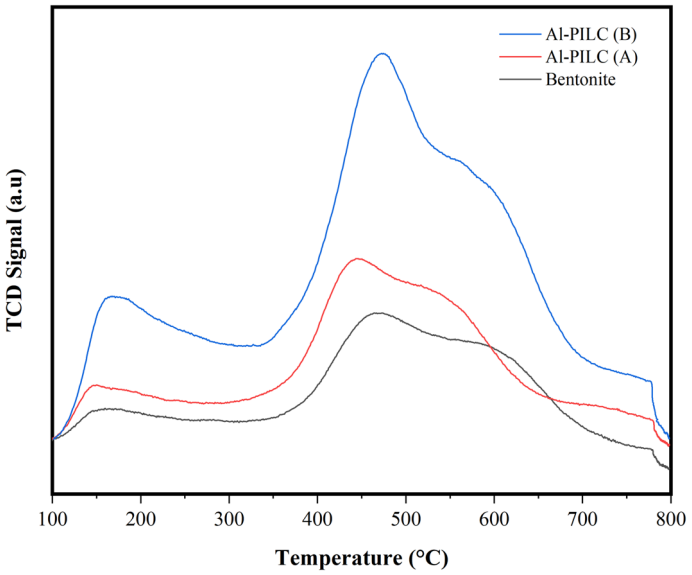

Fig. 5 NH_3-TPD profiles of the catalysts

The acidity results of the prepared catalysts are tabulated in Table 3. The Al-PILC catalyst synthesized by sonochemistry shows a higher acidity value than the Al-PILC synthesized using the conventional method, with a value of 5.269 mmol/g. It can be concluded that the ultrasonication method increases the amount of Al_2O_3 metal intercalated into the layered structure of bentonite through a mechanism involving the exchange of Keggin-ion Al_{13} with other cations present in the interlayer structure of bentonite [54].

The acidity of the catalysts consists of Brønsted and Lewis acids. Brønsted acid in pillared bentonite is generated by the hydroxyl groups of the silanol groups in the layered structure of bentonite. In contrast, the Lewis acid originates from aluminum metal oxide pillars (Al_2O_3). The aluminum metal contributes to the Lewis acid sites by providing an empty 3p orbital to accept lone pair electrons from other atoms or molecules. This suggests that strong acid sites correspond to Brønsted acid sites and their results from the ion exchange between Al^{3+} and H^+ ions. Furthermore, the weak acid sites identified through NH_3-TPD analysis indicate the Lewis acid sites characterized by electron deficiency [54]. Al-PILCs show high values of acid density expressed in mmol NH_3/m^2 specific surface area compared with bentonite because of the increase in the total acidity and BET surface area after the pillarization process.

Pyridine and n-butylamine adsorption have been reported to measure the acidity strength and number in solid acid materials [55, 56]. The total acid number of the samples can be calculated by dividing the total number of acid sites by the moles of adsorbed pyridine or n-butylamine. Pyridine adsorption treatment is used to evaluate the distribution of Brønsted and Lewis acids on the surface, followed by FTIR analysis on the pyridine-adsorbed samples. Vibration spectra of pyridine are shown at 1400–1700 cm^{-1}. Surface hydroxyl groups physically adsorb pyridine in the studied oxide structures. Based on Fig. S7, the absorption bands were observed in the wavenumber region around 1550 cm^{-1} and 1404 cm^{-1}. The absorption peaks around 1550 cm^{-1} correspond to the vibrations of pyridinium ions formed as a result of proton transfer from Brønsted acid sites, while the absorption at 1404 cm^{-1} is attributed to pyridine adsorption on the Lewis acid sites [23, 57]. The Lewis and Brønsted acid

Table 3 Acid properties of the catalysts

Sample	Total acidity (mmol/g)[a]	Weak acidity (mmol/g)[b]	Strong acidity (mmol/g)[c]	Acid density ($mmol/m^2$)[d]	L/B ratio[e]
Bentonite	1.94	0.30	1.63	0.04	1.76
Al-PILC (A)	2.31	0.52	1.78	0.04	1.26
Al-PILC (B)	5.27	1.37	3.90	0.09	1.11

[a]Obtained from NH_3-TPD analysis

[b]Calculated by using the area at 100–300 °C

[c]Calculated by using the area at 300–800 °C

[d]Obtained from total acidity/specific surface area

[e]L value obtained from peak area at 1404–1450 cm^{-1} and B value obtained from peak area at 1550 cm^{-1} from Py-FTIR spectrum

site ratio (L/B) values of each sample can be calculated using the area of the Py-FTIR spectrum at each characteristic wavenumber. Table 3 shows that pillarization with Al_2O_3 decreased the L/B ratio value of bentonite. This phenomenon indicates that the presence of Brønsted acid sites on Al-PILC is more dominant compared to bentonite.

Thermal stability analysis

The TG/DTA curves for the bentonite and Al-PILC catalysts are shown in Fig. 6. As can be seen, bentonite and Al-PILC samples showed similar thermal behavior in which mass loss for all the samples occurs in three stages. The TG curve indicates that at temperatures up to 200 °C, bentonite has lost a percentage of its mass. This mass loss is attributed to the desorption of physically adsorbed water on the surface of bentonite and the release of water molecules bound to exchanged cations in the interlayer spaces of bentonite [58]. Al-PILC showed a mass loss of 7.09% (conventional method) and 5.73% (ultrasonication method) over the same temperature range. The second mass reductions at 200–450 °C for bentonite, Al-PILC (A), and Al-PILC (B) are 14.47%, 8.81%, and 7.12%, respectively. This range of mass reduction temperature is associated with the dehydroxylation of bentonite, which results from hydroxyl groups in the bentonite octahedral layer [59]. Finally, mass loss

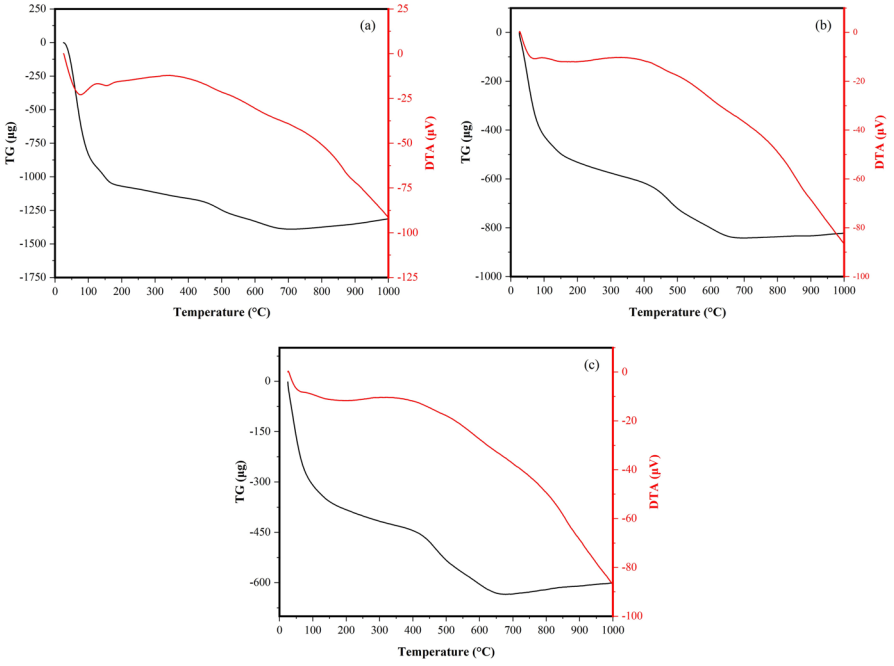

Fig. 6 TG (black)/DTA (red) curves of **a** bentonite, **b** Al-PILC (A), and **c** Al-PILC (B). (Color figure online)

occurring at temperatures ranging from 400 to 700 °C (bentonite = 16.92%, Al-PILC (A) = 11.99%, and Al-PILC (B) = 10.15%) is attributed to the thermal decomposition of the layered pattern of the bentonite clay [60]. This is consistent with the literature, which reports the thermal stability of pillared clays up to 650 °C. This step is related to the stability of the pillars since an essential decrease in the basal spacing values occurs at this temperature, indicating the collapse of the clay structure [61].

On the DTA curve of bentonite and Al-PILCs, endothermic peaks up to 200 °C represent the endothermic reaction of the physically released adsorbed water molecules from the interlayer space of the bentonite structure [51]. The second small peak corresponds to the structural dehydroxylation of the clay mineral [59]. The third low-intensity endothermic peak for Al-PILCs occurred at 400–700 °C, confirming the thermal decomposition of the layered pattern of the bentonite clay [60]. The total mass loss for the bentonite and Al-PILC samples is as follows: bentonite (44.41%), Al-PILC (A) (27.89%), and Al-PILC (B) (23.00%). The pillarization of bentonite with Al_2O_3 enhances the thermal stability of the material. The ultrasonication process yields Al-PILC material with better thermal stability than the conventional method because the intercalation of pillaring agent polyoxocations Al_{13} into the bentonite structure is more extensive, thereby increasing the potential for forming Al_2O_3 pillars.

Catalytic ethanol dehydration into diethyl ether

The ethanol dehydration process leading to diethyl ether formation results in three categories of products: liquid, gas, and solid products in the form of coke. However, this investigation only focuses on liquid products to assess catalyst activity based on the quantity of diethyl ether produced, not other products such as gas and solid. The experiments were conducted using the same catalyst weight, comparing the catalytic performance of all catalysts (bentonite, Al-PILC (A), and Al-PILC (B)) at 225 °C. The results of the catalytic ethanol dehydration using bentonite and Al-PILC catalysts are shown in Fig. 7. The ethanol conversion using the Al-PILC catalysts is higher than that using bentonite. This is because the alumina pillarization process of bentonite catalysts increases the acidity value in the catalyst. The strength of surface acid sites greatly influenced the acidity density of the catalyst material and the synthesis of diethyl ether [62]. The presence of protons (H^+) released by the ionization of strong acids as Brønsted acid sites will protonate ethanol molecules to form ethoxide ions as intermediate compounds in the formation of DEE. The synthesis of Al-PILC using the ultrasonication method yields significantly higher ethanol conversion than Al-PILC synthesized by the conventional method. We can conclude that ultrasonication can increase the catalyst's total acidity value and surface properties, thereby enhancing ethanol conversion. This statement is confirmed by the results of the L/B ratio value of Al-PILC (B), which is lower than Al-PILC (A) and bentonite, so better catalytic performance is obtained for the use of Al-PILC (B).

We define catalyst selectivity as the catalyst's ability to form diethyl ether via ethanol dehydration. Typically, the characteristics of the acid site and the reaction conditions, particularly temperature, influence the catalyst selectivity. Fig. 7 shows

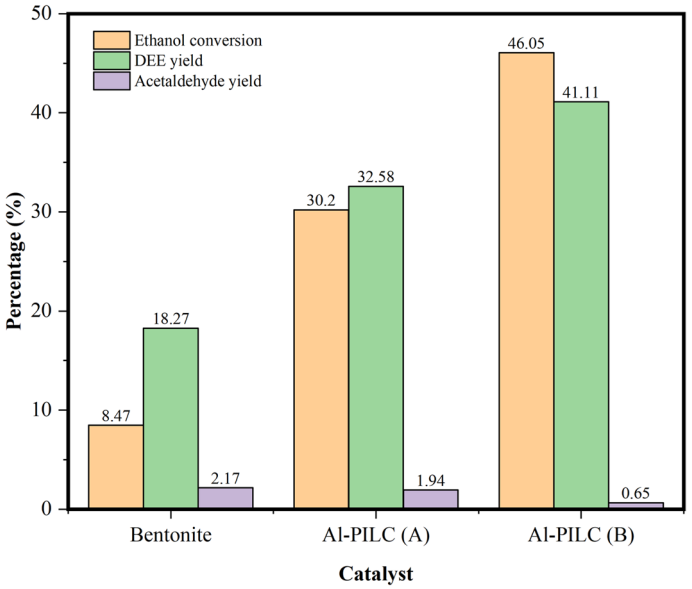

Fig. 7 Histogram of catalytic ethanol dehydration using various catalysts. Experimental conditions: T = 225 °C, N_2 gas flow rate = 20 mL/min, m catalyst = 0.2 g, and V ethanol = 10 mL

that Al-PILC synthesized using the ultrasonication method produces a higher percentage of DEE yield at 41.11% compared with bentonite and Al-PILC synthesized by the conventional method. This result is consistent with the surface characteristics and total acidity of the Al-PILC material synthesized using the sonication method, as indicated in Tables 1 and 3. Based on these data, the catalyst acidity, as confirmed by the NH_3-TPD results, plays an essential role in enhancing the catalytic activity of Al-PILC materials.

In this study, the ethanol dehydration of the Al-PILC (B) catalyst was performed at various reaction temperatures to determine the optimum temperature. The results are presented in Fig. 8. The reaction temperature increase was accompanied by an increase in the conversion of liquid, with conversions at 200, 225, and 250 °C of 13.33, 46.05%, and 48.18%, respectively. The Arrhenius equation shows that a temperature increase would enhance the reaction rate constant, consequently increasing the overall reaction rate. Therefore, increased temperatures can improve ethanol conversion [1, 63, 64].

Fig. 8 shows that the ethanol dehydration over the Al-PILC (B) catalyst occurs at the optimum temperature of 225 °C, with the highest product yield of diethyl ether being 41.11%. Although the highest ethanol conversion occurs at 250 °C, the dehydration reaction produces diethyl ether (18.90%) and generates other by-products, like acetaldehyde, with approximately 4.66%. Furthermore, ethanol dehydration at temperatures exceeding 400 °C will yield up to 100% ethylene [10]. We can conclude that the highest ethanol conversion occurs at 250 °C, whereas the highest selectivity toward diethyl ether is observed at 225 °C. The highest diethyl ether content was obtained, reaching 1.62%, using the SO_4/ZrO_2 catalyst at a reaction

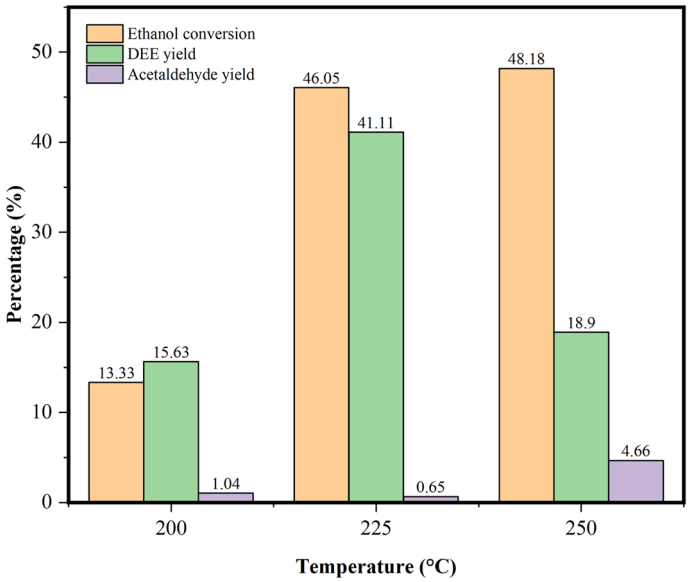

Fig. 8 Histogram of catalytic ethanol dehydration using Al-PILC (B) catalyst at various temperatures. Experimental conditions: N_2 gas flow rate = 20 mL/min, m catalyst = 0.2 g, and V ethanol = 10 mL

temperature of 225 °C [65]. The optimum temperature for ethanol dehydration at 225 °C has also been reported by researchers using different catalysts, such as the SO_4/TiO_2 catalyst [43] and the SO_4/SiO_2 catalyst [64], with diethyl ether yields of 1.72% and 9.54%, respectively.

The reaction pathways for the dehydration of ethanol as stated by Rahmanian and Ghaziaskar [66] are shown in Fig. S8. Typically, ethanol can be converted into higher-value chemical products via a dehydration reaction, such as diethyl ether, acetaldehyde, and ethylene, depending on the reaction temperature when catalytically dehydrated using solid acid catalysts. The diethyl ether and ethylene formation are thermodynamically favored at temperatures ranging from 150 to 350 °C and 350 to 500 °C, respectively [67].

Reusability test of the catalyst

The reusability test of the Al-PILC (B) catalyst was conducted using this catalyst for three consecutive runs, and the results are depicted in Fig. S9. The ethanol conversion of the produced liquid decreases significantly over three runs (46.05%, 21.16%, and 14.32%, respectively). The reduction of ethanol conversion is followed by a decrease in the yield of diethyl ether produced. This decline might be attributed to coking deactivation. Coking refers to the accumulation of carbon deposits on the catalyst surface, covering the catalyst pores after the first run.

Consequently, the catalyst deactivates, resulting in a subsequent decrease in the Al-PILC (B) catalytic activity. SEM image of the Al-PILC (B) catalyst after three

Table 4 Elemental composition obtained by EDX of Al-PILC (B) catalyst after reusability test

Element	Percentage (wt%)
O	45.63
Al	11.82
Si	24.07
Ca	1.06
Mg	1.44
K	0.38
Fe	4.33
C	10.63

consecutive runs in Fig. S10 shows that the catalyst's pore surface is partially covered by carbon deposits, reducing catalyst activity during the conversion of ethanol to diethyl ether. The formation of coke in heterogeneous catalytic reaction processes is highly likely to occur due to the contact and decomposition of organic materials with the solid catalyst at high temperatures [68]. This statement is also supported by the EDX data from the spent Al-PILC (B) catalyst sample presented in Table 4. EDX analysis successfully detected the presence of carbon on the catalyst's surface, which can interfere with the catalyst's performance in repeated use. Future research is necessary to modify Al-PILC (B), such as by dispersing transition metals to minimize catalyst deactivation.

Conclusion

The solid acid catalyst has been successfully synthesized from bentonite through a pillarization process using the Keggin-ion Al_{13}, forming Al-PILC by different intercalation methods, which are the conventional stirring labeled as Al-PILC (A) and the ultrasonication labeled as Al-PILC (B). The difference in the bentonite intercalation stage's synthesis methods affects the Al-PILC catalyst's physicochemical properties. The surface area values of Al-PILC (A) and Al-PILC (B) were 54.54 m^2/g and 60.03 m^2/g, respectively, showing no significant difference. However, a notable increase in total acidity was observed between Al-PILC (A) and Al-PILC (B) due to variations in the intercalation method, with measurements of 2.31 mmol/g and 5.27 mmol/g, respectively. Compared to Al-PILC (A), Al-PILC (B) shows better acidity and surface area values and is more beneficial to green chemistry in the synthesis of Al-PILC.

Consequently, it has enhanced catalytic activity while generating diethyl ether. The optimum reaction temperature of ethanol dehydration over the Al-PILC (B) catalyst is 225 °C, with the highest product yield of diethyl ether being 41.11%. However, the liquid conversion is 46.05% lower than that of Al-PILC (A), which is 48.18%. Further investigation is necessary to determine how catalyst mass and reaction time affect the catalyst activity and selectivity and modifications to it to improve stability when used repeatedly.

Supplementary Information The online version contains supplementary material available at https://doi.org/10.1007/s11144-024-02659-1.

Author contributions Puji Wahyuningsih: Conceptualization, Data curation, Methodology, Software, Visualization, writing—original draft, writing—reviewing & editing. Aldino Javier Saviola: Data curation, Software, Visualization, writing—original draft, writing—reviewing & editing. Karna Wijaya: Conceptualization, Formal analysis, Funding acquisition, Investigation, Methodology, Project administration, Resources, Supervision, Validation, writing—reviewing & editing. Aulia Sukma Hutama: Formal analysis, Investigation, Methodology, Supervision, Validation, writing—reviewing & editing Won-Chun Oh: Formal analysis, Investigation, Supervision, writing—reviewing & editing. Latifah Hauli: Formal analysis, Investigation, Supervision, writing—reviewing & editing.

Funding This research was provided by Penelitian Disertasi Doktor (PDD), Project of Kementerian Pendidikan, Kebudayaan, Riset dan Teknologi (Kemdikbudristek) 2023 with Contract Number 122/E5/PG.02.00.PL/2023;3104/UN1/DITLIT/Dit-Lit/PT.01.03/2023. The authors acknowledge the National Research and Innovation Agency through E-Layanan Sains, Advanced Characterization Laboratories Serpong, LPPT Universitas Gadjah Mada, and their facilities, scientific, and technical assistance.

Data availability The authors declare that the data supporting the findings of this study are available within the paper. Should raw data files be needed in another format, they are available from the corresponding author upon reasonable request.

Declarations

Conflict of interest The authors declare no conflict of interest.

Ethical approval This work contains no studies with human participants or animals performed by the author.

References

1. Autthanit C, Likitpiriya N, Praserthdam P, Jongsomjit B (2021) Development of a new ternary Al_2O_3-HAP-Pd catalyst for diethyl ether and ethylene production using the preferential dehydration of ethanol. ACS Omega 6:19911–19923. https://doi.org/10.1021/acsomega.1c02818
2. Kamsuwan T, Jongsomjit B (2018) Characterization of different Si-and Al-based catalysts with pd modification and their use for catalytic dehydration of ethanol. J Oleo Sci 67:1005–1014. https://doi.org/10.5650/jos.ess18001
3. Abu-Dahrieh J, Rooney D, Goguet A, Saih Y (2012) Activity and deactivation studies for direct dimethyl ether synthesis using CuO-ZnO-Al_2O_3 with NH_4ZSM-5, HZSM-5 or γ-Al_2O_3. Chem Eng J 203:201–211. https://doi.org/10.1016/j.cej.2012.07.011
4. Lee S, Kim TY (2017) Performance and emission characteristics of a DI diesel engine operated with diesel/DEE blended fuel. Appl Therm Eng 121:454–461. https://doi.org/10.1016/j.applthermaleng.2017.04.112
5. Venu H, Madhavan V (2017) Influence of diethyl ether (DEE) addition in ethanol-biodiesel-diesel (EBD) and methanol-biodiesel-diesel (MBD) blends in a diesel engine. Fuel 189:377–390. https://doi.org/10.1016/j.fuel.2016.10.101
6. Alviany R, Wahyudi A, Gunardi I et al (2018) Diethyl ether production as a substitute for gasoline. EDP Sci. https://doi.org/10.1051/matecconf/201815606003
7. de Oliveira TKR, Rosset M, Perez-Lopez OW (2018) Ethanol dehydration to diethyl ether over Cu-Fe/ZSM-5 catalysts. Catal Commun 104:32–36. https://doi.org/10.1016/j.catcom.2017.10.013
8. Singh A, Singh S (2021) Impact of biodiesel–diesel and diethyl ether blends on the performance and emissions of a dual fuel diesel engine. J Inst Eng 102:705–711. https://doi.org/10.1007/s40032-021-00685-9

9. Phung TK, Hernández LP, Busca G (2015) Conversion of Ethanol over transition metal oxide catalysts: effect of Tungsta addition on catalytic behaviour of Titania and zirconia. Appl Catal A Gen 489:180–187. https://doi.org/10.1016/j.apcata.2014.10.025
10. Pratika RA, Wijaya K, Utami M et al (2023) The potency of hydrothermally prepared sulfated silica (SO_4/SiO_2) as a heterogeneous acid catalyst for ethanol dehydration into diethyl ether. Chemosphere. https://doi.org/10.1016/j.chemosphere.2023.139822
11. Wang R, Zhao Z, Gao P et al (2022) Impact of adsorption configurations on alcohol dehydration over alumina catalysts. J Phys Chem C 126:10073–10080. https://doi.org/10.1021/acs.jpcc.2c03303
12. Aneu A, Pratika RA, Hasanudin, et al (2023) Silica-based catalysts for biodiesel production: a brief review. Silicon. https://doi.org/10.1007/s12633-023-02403-9
13. Rinaldi N, Kristiani A (2017) Physicochemical of pillared clays prepared by several metal oxides. Am Inst Phys Inc. https://doi.org/10.1063/1.4978136
14. Basoglu FT, Balci S (2016) Catalytic properties and activity of copper and silver containing Al-pillared bentonite for CO oxidation. J Mol Struct 1106:382–389. https://doi.org/10.1016/j.molstruc.2015.10.072
15. Torres M, de los Santos C, Portugau P et al (2021) Utilization of a PILC-Al obtained from Uruguayan clay as support of mesoporous MnOx-catalysts on the combustion of toluene. Appl Clay Sci. https://doi.org/10.1016/j.clay.2020.105935
16. Rinaldi N, Purba NDE, Kristiani A et al (2023) Bentonite pillarization using sonication in a solid acid catalyst preparation for the oleic acid esterification reaction. Catal Commun. https://doi.org/10.1016/j.catcom.2022.106598
17. Kloprogge JT (2017) Infrared and Raman spectroscopies of pillared clays. Developments in clay science. Elsevier, Amsterdam. https://doi.org/10.1016/B978-0-08-100355-8.00012-6
18. Gil A, Gandía LM, Vicente MA (2000) Recent advances in the synthesis and catalytic applications of pillared clays. Catal Rev Sci Eng 42:145–212. https://doi.org/10.1081/CR-100100261
19. Hasanudin H, Asri WR, Husnia L et al (2023) Catalytic dehydration of 2-propanol over nickel phosphide immobilized on natural bentonite. React Kinet Mech Catal 136:727–740. https://doi.org/10.1007/s11144-023-02373-4
20. Kumar P, Jasra RV, Bhat SGT (1997) Effect of OH-/Al ratio of pillaring solution on the texture and surface acidity of aluminium pillared clays. Indian J Chem 36:667–67
21. Tomlinson AAG (1998) Characterization of pillared layered structures. J Porous Mater 5:259–274
22. Chávez-García ML, de Pablo-Galán L, Saucedo-Ramírez MP (2006) Synthesis of intercalated Al-Hydroxy-montmorillonite. J Mex Chem Soc 50:36–41
23. Fatimah I, Wijaya K (2011) Effect of aluminium content in aluminium pillared montmorillonite on its surface acidity properties. ITB J Sci 43:123
24. Liu J, Wang XQ, Yang BB et al (2018) Highly efficient conversion of glucose into methyl levulinate catalyzed by tin-exchanged montmorillonite. Renew Energy 120:231–240. https://doi.org/10.1016/j.renene.2017.12.104
25. Castro A, Amaya J, Molina R, Moreno S (2020) Pillarization in concentrated media with solid Al and Al-Zr polymers to obtain acid catalysts. Catal Today 356:284–291. https://doi.org/10.1016/j.cattod.2019.04.006
26. Sanabria NR, Molina R, Moreno S (2009) Effect of ultrasound on the structural and textural properties of Al-Fe pillared clays in a concentrated medium. Catal Letters 130:664–671. https://doi.org/10.1007/s10562-009-9956-4
27. Agustian E, Rachmawati A, Purba NDE et al (2021) Effect of ultrasonic treatment on the preparation of zirconia pillared bentonite as a catalyst. J Phys. https://doi.org/10.1088/1742-6596/1951/1/012017
28. González B, Pérez AH, Trujillano R et al (2017) Microwave-assisted pillaring of a montmorillonite with Al-polycations in concentrated media. Materials 10:886. https://doi.org/10.3390/ma10080886
29. Zhou X, Wang C, Chu Y et al (2022) Mechanistic insight into ethanol dehydration over SAPO-34 zeolite by solid-state NMR spectroscopy. Chem Res Chin Univ 38:155–160. https://doi.org/10.1007/s40242-022-1450-1
30. Chen Z, Li J, Cheng Z, Zuo S (2018) Well-defined and highly stable AlNi composite pillared clay supported PdOx nanocrystal catalysts for catalytic combustion of benzene. Appl Clay Sci 163:227–234. https://doi.org/10.1016/j.clay.2018.07.030
31. Sandhya M, Ramasamy D, Sudhakar K et al (2021) Ultrasonication an intensifying tool for preparation of stable nanofluids and study the time influence on distinct properties of graphene nanofluids

– A systematic overview. Ultrason Sonochem 73:105479. https://doi.org/10.1016/j.ultsonch.2021.105479
32. Baloyi J, Ntho T, Moma J (2018) A Novel synthesis method of Al/Cr pillared clay and its application in the catalytic wet air oxidation of phenol. Catal Letters 148:3655–3668. https://doi.org/10.1007/s10562-018-2579-x
33. Aneu A, Wijaya K, Syoufian A (2022) Porous silica modification with sulfuric acids and potassium fluorides as catalysts for biodiesel conversion from waste cooking oils. J Porous Mater 29:1321–1335. https://doi.org/10.1007/s10934-022-01258-6
34. Mason TJ (2002) Uses of power ultrasound in chemistry and processing. Applied sonochemistry. Wiley, Hoboken
35. Sing Yu FW, Ameen M, Aqsha A et al (2021) Effects of ultrasound irradiations time over Ni–Mo/γ-Al_2O_3 catalyst synthesis for 1,3 – Propanediol selectively via aqueous phase reforming of glycerol. Case Studies Chem Environ Eng. https://doi.org/10.1016/j.cscee.2021.100096
36. Barakan S, Aghazadeh V (2021) The advantages of clay mineral modification methods for enhancing adsorption efficiency in wastewater treatment: a review. Environ Sci Pollutan Res 28:2572–2599. https://doi.org/10.1007/s11356-020-10985-9/Published
37. Tomul F (2011) Effect of ultrasound on the structural and textural properties of copper-impregnated cerium-modified zirconium-pillared bentonite. Appl Surf Sci 258:1836–1848. https://doi.org/10.1016/j.apsusc.2011.10.056
38. Marosz M, Kowalczyk A, Chmielarz L (2020) Modified vermiculites as effective catalysts for dehydration of methanol and ethanol. Catal Today. https://doi.org/10.1016/j.cattod.2019.07.003
39. Hasanudin H, Asri WR, Tampubolon K et al (2022) Dehydration isopropyl alcohol to diisopropyl ether over molybdenum phosphide pillared bentonite. Pertanika J Sci Technol 30:1739–1754. https://doi.org/10.47836/pjst.30.2.47
40. Hasanudin H, Asri WR, Putri QU et al (2022) Montmorillonite-zirconium phosphate catalysts for methanol dehydration. Iranian J Catal 12:389–397. https://doi.org/10.30495/IJC.2022.1960655.1942
41. Phung TK, Busca G (2015) Diethyl ether cracking and ethanol dehydration: acid catalysis and reaction paths. Chem Eng J 272:92–101. https://doi.org/10.1016/j.cej.2015.03.008
42. Wahyuningsih P, Wijaya K, Trisunaryanti W et al (2015) Synthesis and application of alumina pillared bentonite catalyst for esterification of acetic acid with different alcohols. Asian J Chem 27:1304–1308. https://doi.org/10.14233/ajchem.2015.17670
43. Wijaya K, Putri AR, Sudiono S et al (2021) Effectively synthesizing so4/tio2 catalyst and its performance for converting ethanol into diethyl ether (DEE). Catalysts 11:1492. https://doi.org/10.3390/catal11121492
44. Arfaoui J, Boudali LK, Ghorbel A, Delahay G (2009) Effect of vanadium on the behaviour of unsulfated and sulfated Ti-pillared clay catalysts in the SCR of NO by NH_3. Catal Today 142:234–238. https://doi.org/10.1016/j.cattod.2008.07.032
45. Grim RE (1953) Clay mineralogy. Soil Sci. https://doi.org/10.1097/00010694-195310000-00009
46. Henao-Aguire PA, MacIás-Quiroga IF, Giraldo-Gómez GI, Sanabria-González NR (2021) Catalytic oxidation of ponceau 4R in aqueous solution using iron-impregnated Al-pillared bentonite: optimization of the process. Bull Chem React Eng Catal 16:491–506. https://doi.org/10.9767/BCREC.16.3.10757.491-506
47. Tomul F (2016) The effect of ultrasonic treatment on iron-chromium pillared bentonite synthesis and catalytic wet peroxide oxidation of phenol. Appl Clay Sci 120:121–134. https://doi.org/10.1016/j.clay.2015.11.007
48. Bineesh KV, Kim DK, Kim MIL, Park DW (2011) Selective catalytic oxidation of H_2S over V_2O_5 supported on TiO_2-pillared clay catalysts in the presence of water and ammonia. Appl Clay Sci. https://doi.org/10.1016/j.clay.2010.12.022
49. Caccamo MT, Mavilia G, Mavilia L et al (2020) Self-assembly processes in hydrated montmorillonite by FTIR investigations. Materials 13:1100. https://doi.org/10.3390/ma13051100
50. Balci S, Tecimer A (2015) Physicochemical properties of vanadium impregnated Al-PILCs: effect of vanadium source. Appl Surf Sci 330:455–464. https://doi.org/10.1016/j.apsusc.2014.12.160
51. Moma J, Baloyi J, Ntho T (2018) Synthesis and characterization of an efficient and stable Al/Fe pillared clay catalyst for the catalytic wet air oxidation of phenol. RSC Adv 8:30115–30124. https://doi.org/10.1039/c8ra05825c
52. Chen K, Li J, Li J et al (2010) Synthesis and characterization of TiO_2-montmorillonites doped with vanadium and/or carbon and their application for the photodegradation of sulphorhodamine B under

UV-vis irradiation. Colloids Surf a Physicochem Eng Asp 360:47–56. https://doi.org/10.1016/j.colsurfa.2010.02.005
53. Khairina NNL, Kristiani A, Widjaya RR, et al (2022) Conversion of fatty acid into biodiesel using solid catalysts of Ti-Zr and Ti-Cr pillared bentonite. In: AIP Conference Proceedings. AIP Publishing. https://doi.org/10.1063/5.0110942
54. Bahranowski K, Włodarczyk W, Wisła-Walsh E et al (2015) [Ti, Zr]-pillared montmorillonite–A new quality with respect to Ti-and Zr-pillared clays. Microporous Mesoporous Mater 202:155–164. https://doi.org/10.1016/j.micromeso.2014.09.055
55. Tyagi B, Chudasama CD, Jasra RV (2006) Characterization of surface acidity of an acid montmorillonite activated with hydrothermal, ultrasonic and microwave techniques. Appl Clay Sci 31:16–28. https://doi.org/10.1016/j.clay.2005.07.001
56. Yurdakoç M, Akçay M, Tonbul Y, Yurdakoç K (1999) Acidity of silica-alumina catalysts by amine titration using Hammett indicators and FT-IR study of pyridine adsorption. Turk J Chem 23:319–328
57. Tomul F, Balci S (2007) Synthesis and characterization of Al-pillared interlayered bentonites. Gazi Univ J Sci 21(1):21–31
58. Martinez JM, Conconi MS, Booth F, Rendtorff NM (2021) High-temperature transformations of Zr-pillared bentonite. J Therm Anal Calorim 145:51–58. https://doi.org/10.1007/s10973-020-09681-0
59. Chae HJ, Nam I-S, Ham SW, Hong SB (2001) Physicochemical characteristics of pillared interlayered clays. Catal Today 68:31–40. https://doi.org/10.1016/S0920-5861(01)00320-0
60. Guerra DL, Airoldi C, Lemos VP, Angélica RS (2008) Adsorptive, thermodynamic and kinetic performances of Al/Ti and Al/Zr-pillared clays from the Brazilian Amazon region for zinc cation removal. J Hazard Mater 155:230–242. https://doi.org/10.1016/j.jhazmat.2007.11.054
61. El Miz M, Salhi S, Chraibi I et al (2014) Characterization and adsorption study of thymol on pillared bentonite. Open J Phys Chem 04:98–116. https://doi.org/10.4236/ojpc.2014.43013
62. Armenta MA, Valdez R, Silva-Rodrigo R, Olivas A (2019) Diisopropyl ether production via 2-Propanol dehydration using supported iron oxides catalysts. Fuel 236:934–941. https://doi.org/10.1016/j.fuel.2018.06.138
63. Sarve DT, Singh SK, Ekhe JD (2022) Ethanol dehydration to diethyl ether over ZSM-5 and β-Zeolite supported Ni–W catalyst. Inorg Chem Commun 139:109397. https://doi.org/10.1016/j.inoche.2022.109397
64. Wijaya K, Malau MLL, Maisari U et al (2021) Synthesis, characterizations and catalysis of sulfated silica and nickel modified silica catalysts for diethyl ether (DEE) production from ethanol towards renewable energy applications. Catalysts 11:1511. https://doi.org/10.3390/catal11121511
65. Septiyaningrum R, Amin AK, Trisunaryanti W, Wijaya K (2022) Synthesis of SO_4/ZrO_2 catalyst and its application in the conversion of ethanol to diethyl ether. Iranian J Catal 12:439–450. https://doi.org/10.30495/ijc.2022.1963196.1948
66. Rahmanian A, Ghaziaskar HS (2013) Continuous dehydration of ethanol to diethyl ether over aluminum phosphate-hydroxyapatite catalyst under sub and supercritical condition. J Supercrit Fluids 78:34–41. https://doi.org/10.1016/j.supflu.2013.03.021
67. Zhang X, Wang R, Yang X, Zhang F (2008) Comparison of four catalysts in the catalytic dehydration of ethanol to ethylene. Microporous Mesoporous Mater 116:210–215. https://doi.org/10.1016/j.micromeso.2008.04.004
68. Liu S, Zhu M, Iqbal M (2020) Research progress on stability of solid acid catalysts. Catal Surv Asia 24:196–206. https://doi.org/10.1007/s10563-020-09305-5

Publisher's Note Springer Nature remains neutral with regard to jurisdictional claims in published maps and institutional affiliations.

Springer Nature or its licensor (e.g. a society or other partner) holds exclusive rights to this article under a publishing agreement with the author(s) or other rightsholder(s); author self-archiving of the accepted manuscript version of this article is solely governed by the terms of such publishing agreement and applicable law.